Appl. Math. Mech. -Engl. Ed., **34**(8), 985–1000 (2013)
DOI 10.1007/s10483-013-1722-6

Applied Mathematics and Mechanics (English Edition)

Transient analysis of diffusive chemical reactive species for couple stress fluid flow over vertical cylinder*

H. P. RANI[1], G. J. REDDY[1], C. N. KIM[2]

(1. Department of Mathematics, National Institute of Technology, Warangal 506004, India;
2. Department of Mechanical Engineering, College of Advanced Technology (Industrial Liaison Research Institute), Kyung Hee University, Gyeonggi-do 446701, Korea)

Abstract The unsteady natural convective couple stress fluid flow over a semi-infinite vertical cylinder is analyzed for the homogeneous first-order chemical reaction effect. The couple stress fluid flow model introduces the length dependent effect based on the material constant and dynamic viscosity. Also, it introduces the biharmonic operator in the Navier-Stokes equations, which is absent in the case of Newtonian fluids. The solution to the time-dependent non-linear and coupled governing equations is carried out with an unconditionally stable Crank-Nicolson type of numerical schemes. Numerical results for the transient flow variables, the average wall shear stress, the Nusselt number, and the Sherwood number are shown graphically for both generative and destructive reactions. The time to reach the temporal maximum increases as the reaction constant K increases. The average values of the wall shear stress and the heat transfer rate decrease as K increases, while increase with the increase in the Sherwood number.

Key words couple stress fluid, chemical reaction, natural convection, vertical cylinder, finite difference method

Chinese Library Classification O175.7, O414.14
2010 Mathematics Subject Classification 78M20, 80A20, 80A32

Nomenclature

Bu,	combined buoyancy ratio parameter;
C',	species concentration;
C,	dimensionless species concentration;
$\overline{C}_{\rm f}$,	dimensionless average skin-friction coefficient;
$C_{\rm f}$,	dimensionless local skin-friction coefficient;
D	binary diffusion coefficient;
$Gr_{\rm C}$,	mass Grashof number;
$Gr_{\rm T}$,	thermal Grashof number;
g,	acceleration due to gravity;
K,	dimensionless chemical reaction parameter;
k,	thermal conductivity;
k_1,	chemical reaction parameter;
$\overline{Nu}$,	dimensionless average Nusselt number;
Nu_X,	dimensionless local Nusselt number;
Pr,	Prandtl number;
R,	dimensionless radial coordinate;
r,	radial coordinate;
r_0,	radius of cylinder;
Sc,	Schmidt number;
$\overline{Sh}$,	dimensionless average Sherwood number;
Sh_X,	dimensionless local Sherwood number;
T',	temperature;
T,	dimensionless temperature;

* Received Feb. 23, 2012 / Revised Feb. 26, 2013
Corresponding author C. N. KIM, Professor, Ph. D., E-mail: cnkim@khu.ac.in

t', time;
t, dimensionless time;
U, V, dimensionless velocity components along the X- and R-directions;
u, v, velocity components along the x- and r-directions;
X, dimensionless axial coordinate;
x, axial coordinate.

Greek symbols

α, thermal diffusivity;
β_{C}, volumetric coefficient of expansion with concentration;
β_{T}, volumetric coefficient of thermal expansion;
η, material constant;
μ, viscosity of the fluid;
ν, kinematic viscosity;
ρ, density.

Subscripts

w, condition on the wall;
i, designate grid point along the X-direction;
∞, free stream condition;
j, designate grid point along the R-direction.

Superscript

n, time step level.

1 Introduction

Natural convection flows along with chemical reaction effects play an important role in the safety of nuclear reactors, combustion systems, and solar collectors and the metallurgical and chemical engineering such as solidification of binary alloys, dispersion of dissolved materials in crystal growth, drying and dehydration operations in chemical and food processing plants, and combustion of atomized liquid fuels. They also fascinate many researchers for their applications in astrophysics. In view of the above applications, attempts are made to study the free convective flow over a vertical cylinder with the first-order homogeneous chemical reaction effects (a reaction is said to be of first-order if the rate of reaction is directly proportional to the concentration itself, e.g., formation of smog[1]).

Apelblat[2], Andersson et al.[3], Chamkha[4], and Ganesan and Rani[5] studied the effects of chemical reactions on the heat and mass transfer coefficients in a boundary layer flow under different conditions. Stokes[6] generalized the classical Newtonian model to include the effects of couple stresses in a way different from that of Eringen[7]. This is one of the several non-Newtonian fluid theories developed in the twentieth century. In the theory, Stokes considered a body enclosing a volume without considering the microstructure of the infinitesimal fluid volume element. The set of all forces acting on an infinitesimal volume element was, in general, assumed to be equivalent to a single resultant force together with a resultant couple. The moment of the couple was assumed to be non-zero. With this assumption, Stokes proposed the theory of couple stress fluids, allowing for the sustenance of couple stresses and the usual stresses. Also, in the theory, the curvature twist rate tensor was proposed based on the pure kinematic aspects of the rotation vector, and the couple stress was defined in terms of this curvature twist rate tensor. Accordingly, in the balance of the linear momentum of the couple stress flow model, the fourth-order derivatives of velocities were involved. Therefore, the separate angular momentum equation need not be considered. These fluids can also sustain the existence of body forces and body couples as usual. The stress tensor was no longer symmetric in this theory. In comparison with other models developed for polar fluids, this couple stress model has been more broadly applied because of its mathematical simplicity. In recent years, the

couple stress fluid flow study has attracted many researchers due to its extensive industrial and scientific applications similar to the micropolar fluids, e.g., squeezing and lubrication[8–11], bio-fluid mechanics[12–13], magnetohydrodynamic (MHD) flows, and synthesis and plasticity of chemical compounds. Umavathi and Malashetty[14] studied the couple stress fluid flow and heat transfer characteristics of Oberbeck convection in a vertical porous stratum. Rani et al.[15] gave the numerical results for the transient natural convective couple stress fluid flow past a vertical cylinder. In the presence of both homogeneous and heterogeneous chemical reactions with the slip condition, Alemayehu and Radhakrishnamacharya[16] studied the dispersion of a solute in the peristaltic motion of a couple stress fluid through a porous medium. They observed that the effective dispersion coefficient increased with the increase in the permeability parameter while decreased with the increases in the homogeneous chemical reaction, the couple stress, and the slip and heterogeneous reaction parameters. In the presence of chemical reactions, recently, Hayat et al.[17] analyzed the transient three-dimensional flow of the couple stress fluid over a stretched surface.

It can be noted, from the past studies, that the transient of a couple stress fluid flow past a heated vertical cylinder with chemical reaction effects has been paid very little attention. Therefore, the present study aims to study the boundary layer region developed by an isothermal vertical cylinder, which is kept in a couple stress fluid with the first-order homogeneous chemical reaction effect. A chemically reactive species is assumed to be emitted from the cylinder surface in a flow field. This species undergoes an isothermal homogeneous chemical reaction and spreads into the couple stress fluid. The concentration distribution of these species in the flow field is to be simulated in this study. The surface temperature and surface concentration are assumed to be higher than those of the ambient fluid. The non-dimensional unsteady nonlinear partial differential equations which govern the momentum, heat, and mass transfer are solved numerically with the help of Thomas and pentadiagonal algorithms. The transient effects of the couple stress fluid based on the flow profiles with time for different non-dimensional numbers are analyzed.

A mathematical description about the problem is given in Section 2. Where mass, momentum, energy, and concentration governing equations are derived and made to be dimensionless. Section 3 deals with the numerical schemes for solving the above unsteady coupled non-linear governing equations. Section 4 details the unsteady nature of the flow variable, the average momentum, and the heat and mass transfer coefficients, and a comparison between the couple stress fluid flow and the Newtonian fluid flow. Finally, the summary of the present work is given in Section 5.

2 Formulation of problem

The combined heat and mass transfer boundary layer flow of a couple stress viscous incompressible fluid past an uniformly heated semi-infinite vertical cylinder with the radius r_0 is considered. The x-axis is measured from the leading edge of the cylinder, where the boundary layer thickness is zero, and is taken along the axis of the cylinder. The radial coordinate r is considered to be perpendicular to the axis of the cylinder. The fluid temperature and concentration that are surrounding the cylinder are assumed to be the ambient temperature T'_∞ and the concentration C'_∞, respectively. Initially ($t' = 0$), the cylinder and the fluid are kept at T'_∞ and C'_∞, respectively. As $t' > 0$, the temperature and concentration of the cylinder are raised to $T'_{\rm w}\,(> T'_\infty)$ and $C'_{\rm w}\,(> C'_\infty)$, respectively. A homogeneous first-order chemical reaction is assumed to exist, and changes the concentration of a species in the flow domain. But the level of the species concentration is assumed to be very low, and in this reaction, the reactive component given off by the surface occurs in a very dilute form. Thus, the heat generated during the chemical reaction is negligible. It is assumed that the effect of the viscous dissipation is negligible in the heat transport equation since the flow velocity magnitude is expected to be small.

In comparison with other chemical species, which are presented in fluids, it is assumed that the diffusing species concentration C' in the binary mixture is very small. Therefore, the interfacial velocity at the cylinder surface due to the mass diffusion process is negligible. With the above assumptions, the governing boundary layer equations with Boussinesq's approximation are as follows:

(i) Conservation of mass

$$\frac{\partial(ru)}{\partial x}+\frac{\partial(rv)}{\partial r}=0. \tag{1}$$

(ii) Conservation of momentum

$$\begin{aligned}&\rho\Big(\frac{\partial u}{\partial t'}+u\frac{\partial u}{\partial x}+v\frac{\partial u}{\partial r}\Big)\\&=\rho g\beta_{\mathrm{T}}(T'-T'_\infty)+\rho g\beta_{\mathrm{C}}(C'-C'_\infty)+\frac{1}{r}\frac{\partial}{\partial r}\Big(\mu r\frac{\partial u}{\partial r}\Big)-\eta\nabla^4 u.\end{aligned} \tag{2}$$

(iii) Energy equation

$$\frac{\partial T'}{\partial t'}+u\frac{\partial T'}{\partial x}+v\frac{\partial T'}{\partial r}=\frac{\alpha}{r}\frac{\partial}{\partial r}\Big(r\frac{\partial T'}{\partial r}\Big). \tag{3}$$

(iv) Species concentration equation

$$\frac{\partial C'}{\partial t'}+u\frac{\partial C'}{\partial x}+v\frac{\partial C'}{\partial r}=\frac{D}{r}\frac{\partial}{\partial r}\Big(r\frac{\partial C'}{\partial r}\Big)-k_1C'. \tag{4}$$

The material constant η, which has the dimension of momentum, and the biharmonic operator ($\nabla^4=\nabla^2\nabla^2$) are included at the right-hand side of Eq. (2) due to the property of the couple stress fluid flow. Usually, the ratio of the material constants η and μ has the dimension of the length square, i.e., r_0^2[18].

Stokes[18] mainly proposed two types of boundary conditions, i.e., the couple stresses vanish on the boundary and the fluid vorticity on the boundary is equal to the rotational velocity of the boundary. The present problem is solved based on the later boundary condition. In view of this, the relevant initial and boundary conditions are given by

$$\begin{cases}t'\leqslant 0\colon u=0, \quad v=0, \quad T'=T'_\infty, \quad C'=C'_\infty \quad \text{for all } x \text{ and } r,\\ t'>0\colon u=0, \quad v=0, \quad T'=T'_{\mathrm{w}}, \quad C'=C'_{\mathrm{w}} \quad \text{at} \quad r=r_0,\\ \qquad\ u=0, \quad v=0, \quad T'=T'_\infty, \quad C'=C'_\infty \quad \text{at} \quad x=0,\\ \qquad\ u\to 0, \quad v\to 0, \quad T'\to T'_\infty, \quad C'\to C'_\infty \quad \text{as} \quad r\to\infty\end{cases} \tag{5}$$

and

$$\frac{\partial u}{\partial r}=\frac{\partial v}{\partial x} \quad \text{at} \quad r=r_0 \quad \text{and} \quad \text{as} \quad r\to\infty. \tag{6}$$

By introducing the dimensionless quantities

$$\begin{cases}X=Gr_{\mathrm{T}}^{-1}\dfrac{x}{r_0}, \quad R=\dfrac{r}{r_0}, \quad U=Gr_{\mathrm{T}}^{-1}\dfrac{ur_0}{\nu}, \quad V=\dfrac{vr_0}{\nu},\\ t=\dfrac{\nu t'}{r_0^2}, \quad T=\dfrac{T'-T'_\infty}{T'_{\mathrm{w}}-T'_\infty}, \quad C=\dfrac{C'-C'_\infty}{C'_{\mathrm{w}}-C'_\infty}, \quad Gr_{\mathrm{T}}=\dfrac{g\beta_{\mathrm{T}}r_0^3(T'_{\mathrm{w}}-T'_\infty)}{\nu^2},\\ Gr_{\mathrm{C}}=\dfrac{g\beta_{\mathrm{C}}r_0^3(C'_{\mathrm{w}}-C'_\infty)}{\nu^2}, \quad Pr=\dfrac{\nu}{\alpha}, \quad Sc=\dfrac{\nu}{D},\\ Bu=\dfrac{Gr_{\mathrm{C}}}{Gr_{\mathrm{T}}}, \quad K=\dfrac{k_1r_0^2}{\nu}, \quad r_0=\Big(\dfrac{\eta}{\mu}\Big)^{\frac{1}{2}},\end{cases} \tag{7}$$

which are explained in the nomenclature in Eqs. (1)–(4), the following equations can be obtained:

$$\frac{\partial U}{\partial X}+\frac{\partial V}{\partial R}+\frac{V}{R}=0, \tag{8}$$

$$\begin{aligned}&\frac{\partial U}{\partial t}+U\frac{\partial U}{\partial X}+V\frac{\partial U}{\partial R}\\&=T+BuC+\Big(\frac{\partial^2 U}{\partial R^2}+\frac{1}{R}\frac{\partial U}{\partial R}\Big)-\Big(\frac{1}{R^3}\frac{\partial U}{\partial R}-\frac{1}{R^2}\frac{\partial^2 U}{\partial R^2}+\frac{2}{R}\frac{\partial^3 U}{\partial R^3}+\frac{\partial^4 U}{\partial R^4}\Big),\end{aligned} \tag{9}$$

$$\frac{\partial T}{\partial t}+U\frac{\partial T}{\partial X}+V\frac{\partial T}{\partial R}=\frac{1}{Pr}\Big(\frac{\partial^2 T}{\partial R^2}+\frac{1}{R}\frac{\partial T}{\partial R}\Big), \tag{10}$$

$$\frac{\partial C}{\partial t}+U\frac{\partial C}{\partial X}+V\frac{\partial C}{\partial R}=\frac{1}{Sc}\Big(\frac{\partial^2 C}{\partial R^2}+\frac{1}{R}\frac{\partial C}{\partial R}\Big)-KC. \tag{11}$$

The corresponding initial and boundary conditions in dimensionless quantities are given by

$$\begin{cases} t\leqslant 0\colon U=0, \quad V=0, \quad T=0, \quad C=0 \quad \text{for all } X \text{ and } R,\\ t>0\colon U=0, \quad V=0, \quad T=1, \quad C=1 \quad \text{at} \quad R=1,\\ \qquad U=0, \quad V=0, \quad T=0, \quad C=0 \quad \text{at} \quad X=0,\\ \qquad U\to 0, \quad V\to 0, \quad T\to 0, \quad C\to 0 \quad \text{as} \quad R\to\infty. \end{cases} \tag{12}$$

Similarly, Eq. (6) in dimensionless quantities is given by

$$\frac{\partial U}{\partial R}=\frac{1}{Gr_{\mathrm{T}}^2}\frac{\partial V}{\partial X} \quad \text{at} \quad R=1 \quad \text{and} \quad \text{as} \quad R\to\infty. \tag{13}$$

3 Solution method

An implicit finite difference scheme of the Crank-Nicolson type is used to solve the unsteady coupled nonlinear equations (8)–(11). The finite difference equations corresponding to Eqs. (8)–(11) are as follows:

$$\begin{aligned}&\frac{U_{i,j}^{n+1}-U_{i-1,j}^{n+1}+U_{i,j}^{n}-U_{i-1,j}^{n}}{2\Delta X}+\frac{V_{i,j}^{n+1}-V_{i,j-1}^{n+1}+V_{i,j}^{n}-V_{i,j-1}^{n}}{2\Delta R}\\&+\frac{V_{i,j}^{n+1}}{1+(j-1)\Delta R}=0,\\&\frac{U_{i,j}^{n+1}-U_{i,j}^{n}}{\Delta t}+\frac{U_{i,j}^{n}}{2\Delta X}(U_{i,j}^{n+1}-U_{i-1,j}^{n+1}+U_{i,j}^{n}-U_{i-1,j}^{n})\\&+\frac{V_{i,j}^{n}}{4\Delta R}(U_{i,j+1}^{n+1}-U_{i,j-1}^{n+1}+U_{i,j+1}^{n}-U_{i,j-1}^{n})\end{aligned} \tag{14}$$

$$= \frac{T_{i,j}^{n+1} + T_{i,j}^{n}}{2} + Bu\Big(\frac{C_{i,j}^{n+1} + C_{i,j}^{n}}{2}\Big) + \frac{U_{i,j+1}^{n+1} - U_{i,j-1}^{n+1} + U_{i,j+1}^{n} - U_{i,j-1}^{n}}{4(1+(j-1)\Delta R)\Delta R}$$
$$+ \frac{U_{i,j-1}^{n+1} - 2U_{i,j}^{n+1} + U_{i,j+1}^{n+1} + U_{i,j-1}^{n} - 2U_{i,j}^{n} + U_{i,j+1}^{n}}{2(\Delta R)^2}$$
$$- (U_{i,j+2}^{n+1} - 4U_{i,j+1}^{n+1} + 6U_{i,j}^{n+1} - 4U_{i,j-1}^{n+1} + U_{i,j-2}^{n+1} + U_{i,j+2}^{n}$$
$$- 4U_{i,j+1}^{n} + 6U_{i,j}^{n} - 4U_{i,j-1}^{n} + U_{i,j-2}^{n})/(2(\Delta R)^4)$$
$$- \frac{U_{i,j+2}^{n+1} - 2U_{i,j+1}^{n+1} + 2U_{i,j-1}^{n+1} - U_{i,j-2}^{n+1} + U_{i,j+2}^{n} - 2U_{i,j+1}^{n} + 2U_{i,j-1}^{n} - U_{i,j-2}^{n}}{2(1+(j-1)\Delta R)(\Delta R)^3}$$
$$+ \frac{U_{i,j-1}^{n+1} - 2U_{i,j}^{n+1} + U_{i,j+1}^{n+1} + U_{i,j-1}^{n} - 2U_{i,j}^{n} + U_{i,j+1}^{n}}{2(1+(j-1)\Delta R)^2(\Delta R)^2}$$
$$- \frac{U_{i,j+1}^{n+1} - U_{i,j-1}^{n+1} + U_{i,j+1}^{n} - U_{i,j-1}^{n}}{4(1+(j-1)\Delta R)^3\Delta R}, \tag{15}$$

$$\frac{T_{i,j}^{n+1} - T_{i,j}^{n}}{\Delta t} + \frac{U_{i,j}^{n}}{2\Delta X}(T_{i,j}^{n+1} - T_{i-1,j}^{n+1} + T_{i,j}^{n} - T_{i-1,j}^{n})$$
$$+ \frac{V_{i,j}^{n}}{4\Delta R}(T_{i,j+1}^{n+1} - T_{i,j-1}^{n+1} + T_{i,j+1}^{n} - T_{i,j-1}^{n})$$
$$= \frac{T_{i,j-1}^{n+1} - 2T_{i,j}^{n+1} + T_{i,j+1}^{n+1} + T_{i,j-1}^{n} - 2T_{i,j}^{n} + T_{i,j+1}^{n}}{2Pr(\Delta R)^2}$$
$$+ \frac{T_{i,j+1}^{n+1} - T_{i,j-1}^{n+1} + T_{i,j+1}^{n} - T_{i,j-1}^{n}}{4Pr(1+(j-1)\Delta R)\Delta R}, \tag{16}$$

$$\frac{C_{i,j}^{n+1} - C_{i,j}^{n}}{\Delta t} + \frac{U_{i,j}^{n}}{2\Delta X}(C_{i,j}^{n+1} - C_{i-1,j}^{n+1} + C_{i,j}^{n} - C_{i-1,j}^{n})$$
$$+ \frac{V_{i,j}^{n}}{4\Delta R}(C_{i,j+1}^{n+1} - C_{i,j-1}^{n+1} + C_{i,j+1}^{n} - C_{i,j-1}^{n})$$
$$= \frac{C_{i,j-1}^{n+1} - 2C_{i,j}^{n+1} + C_{i,j+1}^{n+1} + C_{i,j-1}^{n} - 2C_{i,j}^{n} + C_{i,j+1}^{n}}{2Sc(\Delta R)^2}$$
$$+ \frac{C_{i,j+1}^{n+1} - C_{i,j-1}^{n+1} + C_{i,j+1}^{n} - C_{i,j-1}^{n}}{4Sc(1+(j-1)\Delta R)\Delta R} - \frac{K}{2}(C_{i,j}^{n+1} + C_{i,j}^{n}). \tag{17}$$

To solve these equations, the region of integration is considered as a rectangle composed of the lines, indicating

$$X_{\min} = 0, \quad X_{\max} = 1, \quad R_{\min} = 1, \quad R_{\max} = 31,$$

where $R_{\max}$ corresponds to $R = \infty$ which lies very far from the momentum, energy, and concentration boundary layers. In Eqs. (14)–(17), the subscripts i and j designate the grid points along the X- and R-coordinates, respectively, where

$$X = i\Delta X, \quad R = 1 + (j-1)\Delta R,$$

and the superscript n implies the time step along the time t, where $t = n\Delta t$. Here, ΔX, ΔR, and Δt denote the mesh sizes in the X- and R-coordinates and along the time t, respectively. To obtain an economical and reliable grid system for the computations, a grid independency test is performed and shown in Fig. 1. The steady-state velocity, temperature, and concentration values obtained with the grid system of 100×500 differ in the second decimal place from those with the grid system of 50×250, and differ in the fifth decimal place from those with the grid system of $200 \times 1\,000$. Therefore, the grid system of 100×500 is selected for all subsequent analyses with the mesh sizes in the X- and R-directions being 0.01 and 0.06, respectively. Also, the time step size dependency has been tested, from which $\Delta t = 0.01$ has been obtained to be able to get a reliable result.

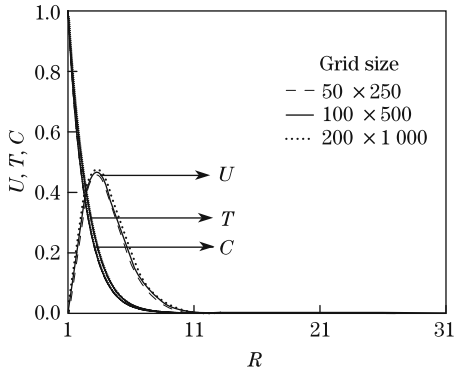

Fig. 1 Grid independency test for velocity, temperature, and concentration profiles with $Pr = 0.7$, $Sc = 0.6$, $Bu = 1.0$, and $K = 0.2$

The numerical procedure starts by solving the heat transport and concentration equations (16)–(17), which provides the temperature and concentration fields, respectively. Then, the solution to the momentum and continuity equations (15) and (14) provides the solution of the velocity. Equations (15)–(17) at the $(n+1)$th iteration are given in the following tridiagonal and pentadiagonal forms:

$$a_{i,j}\phi_{i,j-1}^{n+1} + b_{i,j}\phi_{i,j}^{n+1} + c_{i,j}\phi_{i,j+1}^{n+1} = d_{i,j}, \tag{18}$$

$$A_{i,j}\psi_{i,j-2}^{n+1} + B_{i,j}\psi_{i,j-1}^{n+1} + C_{i,j}\psi_{i,j}^{n+1} + D_{i,j}\psi_{i,j+1}^{n+1} + E_{i,j}\psi_{i,j+2}^{n+1} = F_{i,j}, \tag{19}$$

where ϕ represents the dependent variables T and C, and ψ represents the velocity U. Therefore, Eqs. (18) and (19) on a particular i-level at every internal nodal point constitute a tridiagonal and pentadiagonal system of equations. The solution of such a system of equations was obtained by Thomas[19] and pentadiagonal algorithms[20]. Explicitly, the velocity U is calculated from Eq. (14). Until the convergence of 10^{-5} has been reached, the processes are repeated for consecutive i-levels with many times of sweeping.

4 Results and discussion

For the validation, the temperature and concentration profiles of Newtonian fluids obtained by the current numerical procedure are compared with the existing results of Chen and Yuh[21] for

$$Sc = 0.2, \quad Pr = 0.7, \quad Bu = 1.0, \quad K = 0.0.$$

The current results are found to be in good agreement with the previous results as shown in Fig. 2.

In the present study, attention is paid to the homogeneous first-order chemical reaction parameter K, which has the dimension of the reciprocal of time. The diffusing species can be either destroyed or generated in the homogenous reaction. The couple stress fluid flows with the chemical reaction are of great physical interest, and are to be treated as described below. The finite difference equation (17) can be adjusted to meet these situations if one takes (i) $K > 0$ for the destructive reaction and (ii) $K < 0$ for the generative reaction. Numerical analysis is carried out for different K with $Sc = 0.6$ (water vapour) and 5.0 for $Pr = 0.7$ (air) and $Bu = 1.0$. The obtained transient behavior of the dimensionless velocity, temperature, concentration, average skin-friction coefficient, and heat and mass transfer rates are discussed in detail in the succeeding subsections.

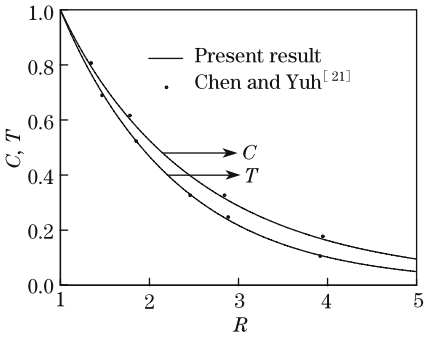

Fig. 2 Comparison of temperature and concentration profiles for Newtonian fluids with $Sc = 0.2$, $Pr = 0.7$, $Bu = 1.0$, and $K = 0.0$

4.1 Velocity

The obtained transient velocity U at (1, 3.28) against t is shown in Fig. 3(a). Here, it is observed that at the beginning, the velocity increases with time, reaches a temporal maximum, then decreases, and at last reaches the asymptotic steady-state for both generative ($K < 0$) and destructive ($K > 0$) reactions. At very early time (i.e., $t \ll 1$), the heat transfer is dominated by conduction. Shortly later, there exists a period when the convective heat transfer rate becomes meaningful with the increase in the upward velocity. When this transient period is almost ending and just before the steady-state is about to be reached, there exist overshoots for the velocities. For a generative reaction, it is observed that the time required to reach the steady-state increases as K decreases since the decrease in K yields an increase in the concentration, which gives an increase in the value of BuC in Eq. (9), resulting in an increased acceleration of the upward flow and a longer time to get the steady-state. However, the opposite trend is observed for the destructive reaction.

Figure 3(b) shows the simulated steady-state velocity profiles against R at X=1.0, where the velocity profiles start with the zero value at the wall, reach their maxima, and then monotonically decrease to zero along the radial coordinate for all t. From Fig. 3(b), it can be observed that the velocity profiles reach their maximum values approximately at (1, 3.28). It is seen that for both generative and destructive reactions, the velocity magnitude decreases with an increase in K since the increase in K yields lower concentration near the wall (see Eq. (11)), and it tends to decelerate the upward flow in association with the term BuC in the right-hand side of Eq. (9).

It can be noted that the velocity decreases with an increase in Sc because the larger Sc is, the smaller the concentration diffusion is, which yields a steeper concentration distribution near the wall and that the concentration boundary layer is thinner than the velocity boundary layer. Therefore, except in a region very near the wall, the value of BuC in Eq. (9) becomes

very small, and it yields small acceleration for the upward velocity, resulting in a small velocity. It is also noticed that the thickness of the velocity boundary layer increases with a decrease in K for a generative reaction, while decreases with a decrease in K for a destructive reaction. The reason is that in the generative reaction, the upward velocity gets a higher acceleration term BuC in Eq. (9), but in the destructive system, the value of BuC is small.

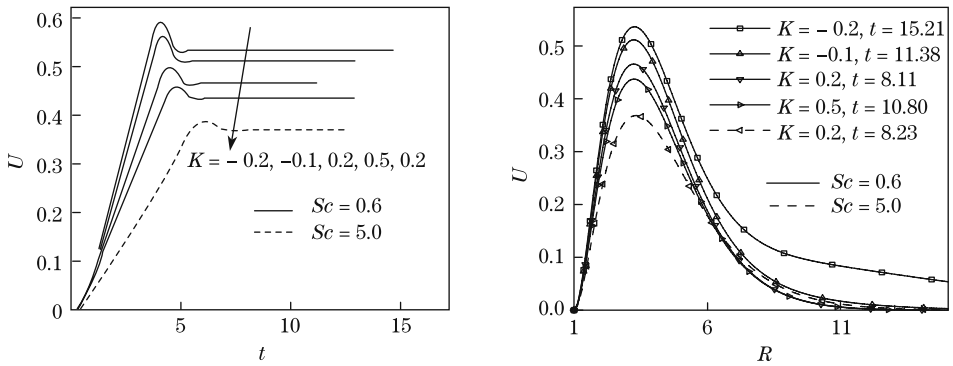

(a) Transient velocity at (1, 3.28) (b) Steady-state velocity at X=1.0

Fig. 3 Simulated transient velocity at (1, 3.28) and steady-state velocity at $X = 1.0$

4.2 Temperature

The obtained transient temperature T with respect to t is shown at the point (1, 1.24) in Fig. 4(a). Here, it is observed that at the beginning, the temperature profiles increase with time, reach the temporal maxima, then decrease, and, again after a slight increase, attain the steady-state asymptotically. The temperatures at other locations also exhibit somewhat similar transient behaviors. Here, it is seen that the steady temperature value decreases with the decrease in K for a fixed Sc. It comes from the fact that the decrease in K gives an increase in the concentration, and, in turn, yields an increase in the upward velocity (see Eq. (9)), yielding the decrease in the temperature near the wall.

The simulated steady-state temperature profiles at $X = 1.0$ against the radial coordinate are shown in Fig. 4(b). The temperature profiles start with the hot wall temperature ($T = 1$), and then monotonically decrease to zero along the radial coordinate. As seen before, a decrease in K yields a decrease in the temperature. Also, the time taken for the temperature to reach the steady-state increases as K decreases for a generative reaction, while decreases as K decreases for a destructive reaction. It is also observed that the temperature increases as Sc increases since a larger Sc means that the concentration diffusion is limited so that a higher concentration is observed only near the wall and a lower concentration is seen in almost all the flow domains,

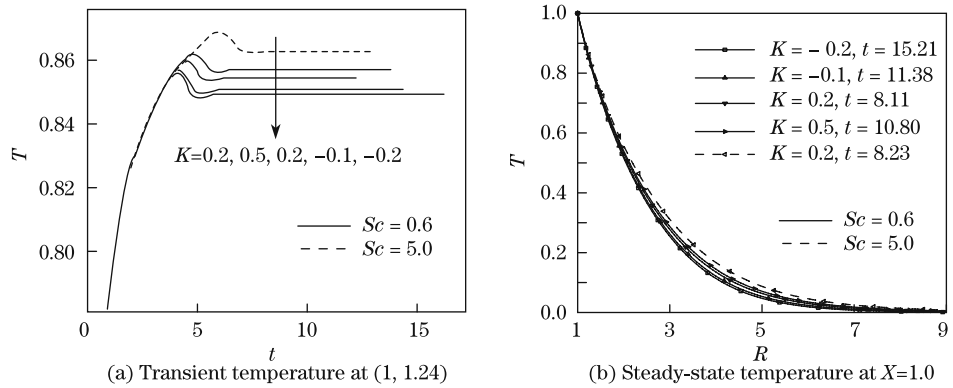

(a) Transient temperature at (1, 1.24) (b) Steady-state temperature at X=1.0

Fig. 4 Simulated transient temperature at (1, 1.24) and steady-state temperature at $X = 1.0$

which gives slower upward flow and yields higher temperature.

4.3 Concentration

The obtained transient concentration C at the point (1, 1.36) against t is shown in Fig. 5(a), where the concentration profiles increase with time at the beginning, reach the temporal maxima, then decrease and increase again, and after a slight increase, attain the steady-state asymptotically. It is observed that the temporal maximum is attained at an early state for smaller K. Also, the time required for the concentration to reach the steady-state increases as Sc increases for fixed K. The concentrations at other locations also exhibit somewhat similar transient behaviors. Here, it is seen that the steady concentration decreases with the increase in K for a fixed Sc since larger K means lower concentration in the flow domain in Eq. (11).

The steady-state concentration profiles at $X = 1.0$ along the radial direction are shown in Fig. 5(b). The concentration profiles start with the wall concentration ($C = 1$), and then monotonically decrease to zero along R. As Sc increases, the concentration diffusion decreases and, as explained before, the concentration profiles decrease. This is in association with the fact that a larger Sc corresponds to a thinner concentration boundary layer relative to the momentum boundary layer. This results in a larger concentration gradient very near the cylinder. For both generative and destructive reactions, as the reaction parameter increases, the concentration profiles decrease. Also, it is observed that for a generative reaction, as K decreases, the thickness of the concentration boundary layer increases away from the hot wall. As K decreases, the concentration increases (see Eq. (11)). Therefore, the term of BuC in Eq. (9) increases in the flow field, yielding an increased velocity. This type of phenomena will be more notable with smaller Sc when the concentration diffusion is more meaningful.

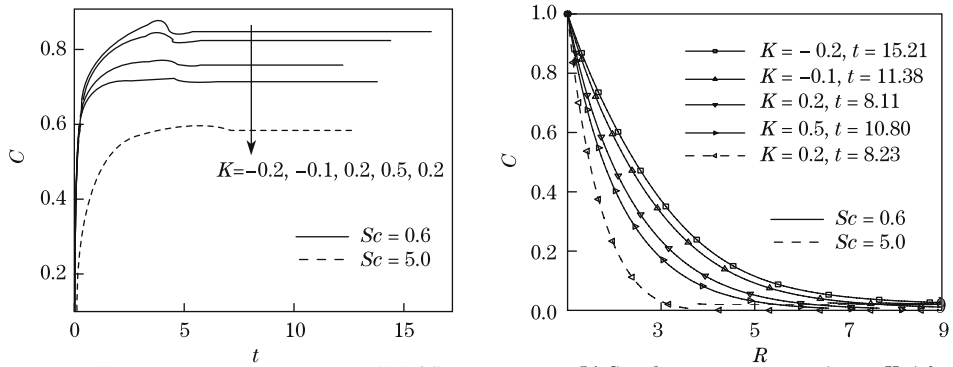

(a) Transient concentration at (1, 1.36) (b) Steady-state concentration at X=1.0

Fig. 5 Simulated transient concentration at (1, 1.36) and steady-state concentration at $X = 1.0$

4.4 Average skin-friction coefficient and heat and mass transfer rates

For engineering practices, the values of the skin-friction coefficient and the heat and mass transfer rate are meaningful. The friction coefficient is an important parameter in the evaluation of heat and mass transfer since it is closely related to the heat and mass transfer coefficients. The increased skin friction is generally a handicap in many technical applications. However, the increased heat and mass transfer can be exploited in some applications such as heat and mass exchangers, but should be avoided in other situations such as gas turbine applications. For the present problem, the skin-friction coefficient and the heat and mass transfer rates are to be derived.

The wall shear stress at the wall can be denoted as

$$\tau_{\mathrm{w}} = \left(\mu \frac{\partial u}{\partial r}\right)_{r=r_0}. \tag{20}$$

By introducing the dimensionless quantities given in Eq. (7), Eq. (20) can be rewritten as

$$\tau_{\mathrm{w}} = \frac{\mu^2 Gr_{\mathrm{T}}}{\rho r_0^2}\Big(\frac{\partial U}{\partial R}\Big)_{R=1}. \tag{21}$$

Regarding $\frac{\mu^2 Gr_{\mathrm{T}}}{\rho r_0^2}$ as the characteristic shear stress, the local skin-friction coefficient can be expressed as

$$C_{\mathrm{f}} = \Big(\frac{\partial U}{\partial R}\Big)_{R=1}. \tag{22}$$

The average skin-friction coefficient can be obtained with the integration of the above equation from

$$X = 0 \quad \text{to} \quad X = 1,$$

which can be written as

$$\overline{C}_{\mathrm{f}} = \int_0^1 \Big(\frac{\partial U}{\partial R}\Big)_{R=1} \mathrm{d}X. \tag{23}$$

The local Nusselt number is given by

$$Nu_x = \frac{\dot{q}_{\mathrm{w}} r_0}{k(T'_{\mathrm{w}} - T'_{\infty})}, \tag{24}$$

where the heat transfer $\dot{q}_{\mathrm{w}}$ is expressed by

$$\dot{q}_{\mathrm{w}} = -k\Big(\frac{\partial' T}{\partial r}\Big)_{r=r_0}.$$

Thus, with the dimensionless quantities introduced in Eq. (7), Eq. (24) can be written as

$$Nu_X = -\Big(\frac{\partial T}{\partial R}\Big)_{R=1}. \tag{25}$$

The following average Nusselt number can be obtained by the integration of Eq. (25) with respect to X from $X = 0$ to $X = 1$:

$$\overline{Nu} = -\int_0^1 \Big(\frac{\partial T}{\partial R}\Big)_{R=1} \mathrm{d}X. \tag{26}$$

The Sherwood number can be written as follows:

$$Sh_x = \frac{\dot{m}_{\mathrm{w}} r_0}{D(C'_{\mathrm{w}} - C'_{\infty})}, \tag{27}$$

where the mass transfer rate $\dot{m}_{\mathrm{w}}$ is given by

$$\dot{m}_{\mathrm{w}} = -D\Big(\frac{\partial C'}{\partial r}\Big)_{r=r_0}.$$

In the same way, Eq. (27) can be transformed to

$$Sh_X = -\Big(\frac{\partial C}{\partial R}\Big)_{R=1}. \tag{28}$$

The following average Sherwood number can be obtained with the integration of Eq. (28) with respect to X:

$$\overline{Sh} = -\int_0^1 \Big(\frac{\partial C}{\partial R}\Big)_{R=1} \mathrm{d}X. \tag{29}$$

The integrations expressed in Eqs. (23), (26), and (29) are evaluated, and the average non-dimensional skin-friction coefficient and the heat and mass transfer rates for couple stress fluids are plotted against the time in Figs. (6)–(8) for different parameters, respectively.

The effects of K on the average skin-friction coefficient are shown in Fig. 6, where for all K, the average skin-friction coefficients increase with time at the beginning, attain the peak values, and then after a slight decrease, reach the asymptotically steady-state. It is also seen that for increasing values of K, the average skin-friction coefficient decreases. This result lies in the same line with the velocity profiles plotted in Fig. 3. Also, it is noticed that the average skin-friction decreases with the increase in Sc, which can be explained in the same line.

Figure 7 shows the effects of K on the average heat transfer rate, revealing that it has the same trend as the average skin-friction with respect to Sc. It is observed that during an earlier period of time, the average Nusselt numbers are almost the same for various parameters, which shows that the initially heat conduction is dominant. In the steady-state, the average heat transfer rate increases as K decreases in both the generative and destructive reactions. Decreasing K speeds up the spatial decay of the temperature near the heated surface because of the increased flow velocity near the wall, yielding an increase in the rate of heat transfer.

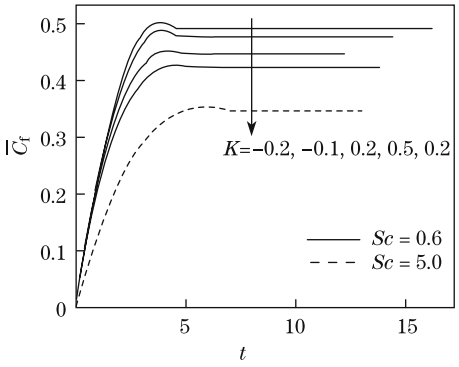

Fig. 6 Simulated average skin-friction

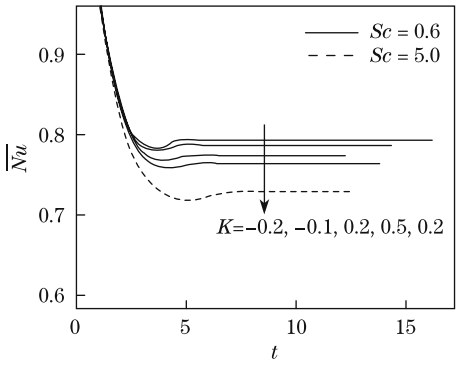

Fig. 7 Simulated average Nusselt number

Figure 8 shows that during an earlier period of time, the mass diffusion is prevailing so that, for a fixed Sc, the average Sherwood numbers are almost the same for different values of K. Generally, in a steady-state, the Sherwood number increases with an increase in K since the increase in K means the decrease in the concentration in the flow field, yielding an increase

in the slope of the concentration distribution along the radial direction. Also, it is observed that the average mass transfer rate increases with the increase in Sc, which is in line with the increase in the concentration slope in Fig. 5(b).

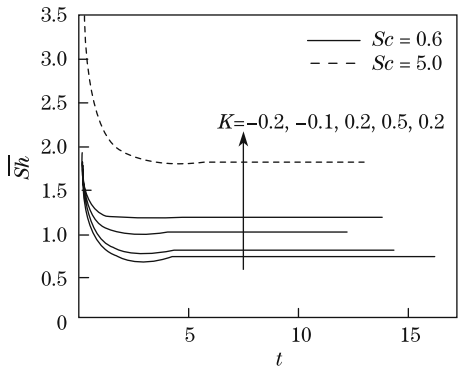

Fig. 8 Simulated average Sherwood number

4.5 Comparison between couple stress and Newtonian fluids

Figure 9 illustrates the steady-state velocity U, temperature T, and concentration C contours for couple stress and Newtonian fluid flows with fixed $Sc = 0.6$ and $K = 0.2$, where the velocity of the couple stress fluid is smaller compared with that of the Newtonian fluid. This is due to the fact that in couple stress fluid flows, there are additive diffusion terms (biharmonic terms)

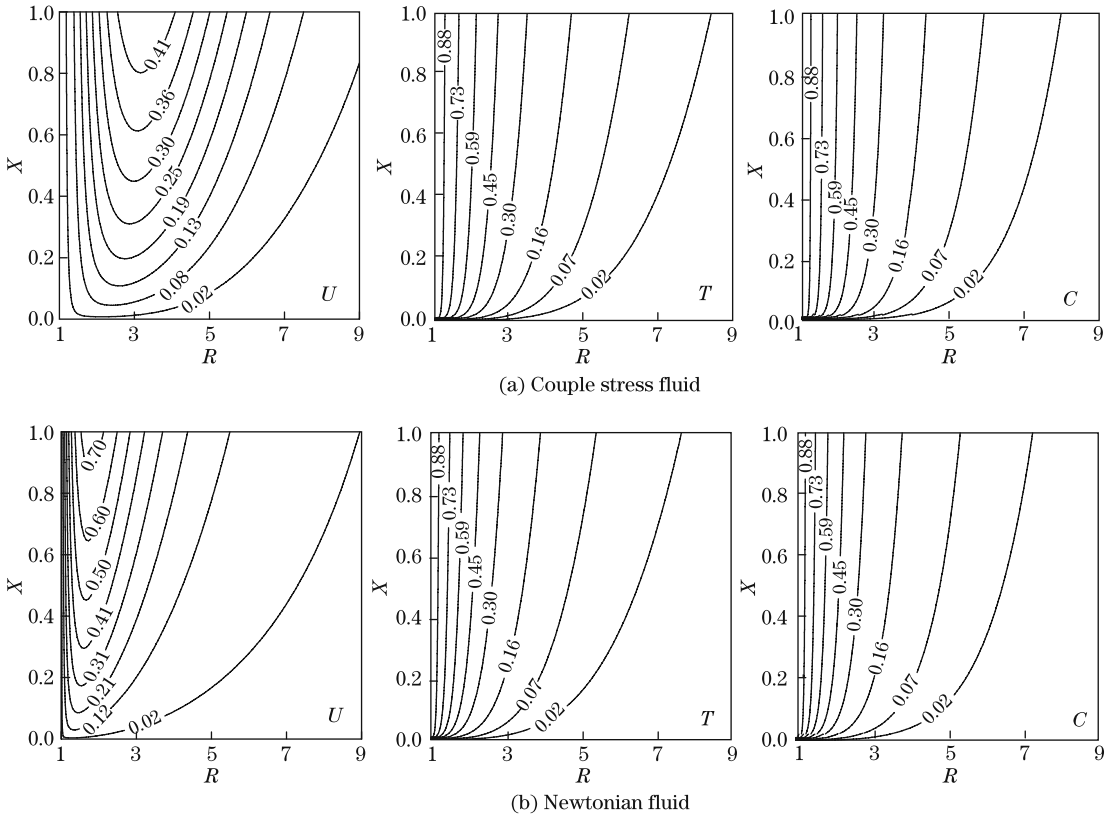

Fig. 9 Steady-state velocity, temperature, and concentration contours with $Sc = 0.6$ and $K = 0.2$

compared with Newtonian fluids (see Eq. (9)). Also, from Figs. 9(a) and 9(b), it is observed that the steady-state velocity, temperature, and concentration of the couple stress fluid are much different from those of the Newtonian fluid, which can be of importance in the study of the behaviors of the couple stress fluids.

Table 1 compares the couple stress fluid flow with the Newtonian fluid flow in terms of the time for the flow variables U, T, and C to reach the temporal maximum and the steady-state time with different reaction constants K and $Sc = 0.6$ and 5.0, where (a) tabulates the values for the couple stress fluid and (b) is for the Newtonian fluid. From (a), it is observed that for all the flow variables, the time required to reach the temporal maximum increases with the increases in K and Sc. From Table 1, it is noticed that the time for all the flow variables to reach the temporal maximum for the couple stress fluid is larger than those for the Newtonian fluid. It is also noticed that the time required for all the flow variables to reach the steady-state and maximum velocity occurring at $X = 1.0$ for the couple stress fluid is smaller than that for the Newtonian fluid.

Table 1 Time to reach temporal maxima of flow variables, steady-state, and maximum velocity at $X = 1.0$ with different K and Sc for (a) couple stress fluid and (b) Newtonian fluid

		K	Temporal maximum			Steady-state	Maximum velocity at $X = 1.0$
			U	T	C		
(a)	$Sc = 0.6$	−0.2	4.07	4.09	3.82	15.21	0.536 2
		−0.1	4.19	4.22	3.89	11.38	0.511 6
		0.2	4.50	4.53	4.09	8.11	0.465 6
		0.5	4.81	4.82	4.25	10.80	0.437 1
	$Sc = 5.0$	0.2	6.06	5.95	5.78	8.23	0.368 3
(b)	$Sc = 0.6$	−0.2	2.71	2.47	2.32	24.23	0.777 1
		−0.1	2.73	2.50	2.33	18.12	0.750 2
		0.2	2.79	2.55	2.34	8.24	0.741 5
		0.5	2.82	2.58	2.36	13.72	0.725 7
	$Sc = 5.0$	0.2	2.84	2.63	2.48	8.47	0.558 0

Table 2 demonstrates the comparison of the couple stress fluid and the Newtonian fluid in terms of the average skin-friction coefficient and the average heat and mass transfer rates with different values of K and $Sc = 0.6$ and 5.0, where (a) shows the values for the couple stress

Table 2 Average skin-friction coefficient, Nusselt number, and Sherwood number with different K and Sc for (a) couple stress fluid and (b) Newtonian fluid

		K	$\overline{C}_{\mathrm{f}}$	$\overline{Nu}$	$\overline{Sh}$
(a)	$Sc = 0.6$	−0.2	0.489 0	0.791 6	0.614 4
		−0.1	0.476 2	0.785 8	0.685 7
		0.2	0.445 7	0.773 4	0.870 5
		0.5	0.423 7	0.764 2	1.022 1
	$Sc = 5.0$	0.2	0.348 0	0.729 2	1.583 7
(b)	$Sc = 0.6$	−0.2	1.703 3	0.958 6	0.866 1
		−0.1	1.621 4	0.940 2	0.921 4
		0.2	1.403 9	0.919 1	1.056 2
		0.5	1.230 0	0.885 7	1.176 0
	$Sc = 5.0$	0.2	1.132 4	0.782 4	1.914 4

fluid and (b) is for the Newtonian fluid. From Table 2, it is observed that the average skin-friction coefficient, the Nusselt number, and the Sherwood number of the couple stress fluid are smaller than those of the Newtonian fluid for all values of K and Sc. This shows that the heat and mass transfer characteristics of the couple stress fluid differ much from those of the Newtonian fluids.

5 Conclusions

A numerical study is carried out for the transient natural convection boundary layer flow of a couple stress, viscous, incompressible fluid over a semi-infinite heated vertical cylinder with the first-order homogeneous chemical reaction effects. The governing equations are derived and normalized based on the length dependent effect introduced by the couple stress fluid flow where the biharmonic operator is involved. A Crank-Nicolson type of implicit methods is used to solve the system of coupled governing equations. Thomas and pentadiagonal algorithms are employed to treat the discretized equations. The computations are carried out for the generative and destructive reactions for two different values of Sc with fixed Pr and Bu.

From the present study, it is obtained that the time required for the velocity, temperature, and concentration profiles to reach the temporal maximum increases with the increase in K. For a generative reaction, it is seen that as K increases, the velocity and the concentration decrease while the temperature increases. Also, it is observed that with the increase in K, the boundary layer thicknesses of the velocity and concentration decrease while the boundary layer thickness of temperature increases. For the destructive reaction, it is noticed that as K decreases, the velocity and the concentration increase, the temperature decreases, and the time taken to reach the steady-state increases. The opposite trend is observed for the generative reaction. As Sc increases, the velocity and the concentration decrease while the temperature increases. As K increases for both the generative and the destructive reactions, the average values of the skin-friction coefficient and the Nusselt number decrease, while the average value of the Sherwood number increases. It is also observed that as Sc increases, the average skin-friction coefficient and the average heat transfer rate decrease, while the average mass transfer rate increases. Particularly, this study reveals that the results pertaining to the couple stress fluid differ significantly from those of the Newtonian fluid. The deviations of the velocity, temperature, and concentration profiles of the couple stress fluid flow from those of the Newtonian fluid flow turn out to be considerable.

As the present study deals only with laminar flows, this work can be extended to the studies on turbulent flows. The body forces like electromagnetic force arising from the MHD flows and the body couples arising in the momentum equation due to the couple stress fluid can be taken into the consideration. Also, the present model can be expanded into the studies of flow past plates, wedges, cones, spheres, etc. based on required applications.

References

[1] Cussler, E. L. *Diffusion Mass Transfer in Fluid Systems*, Cambridge University Press, London (1988)

[2] Apelblat, A. Mass transfer with a chemical reaction of the first order: effects of axial diffusion. *Chemical Engineering Journal*, **23**, 193–203 (1982)

[3] Andersson, H. I., Hansen, O. R., and Holmedal, B. Diffusion of a chemically reactive species from a stretching sheet. *International Journal of Heat and Mass Transfer*, **37**, 659–664 (1994)

[4] Chamkha, A. J. MHD flow of a uniformly stretched vertical permeable surface in the presence of heat generation/absorption and a chemical reaction. *International Communications in Heat and Mass Transfer*, **30**, 413–422 (2003)

[5] Ganesan, P. and Rani, H. P. On diffusion of chemically reactive species in convective flow along a vertical cylinder. *Chemical Engineering and Processing*, **39**, 93–105 (2000)

[6] Stokes, V. K. Couple stress in fluids. *Physics of Fluids*, **9**, 1709–1715 (1966)

[7] Eringen, A. C. Theory of micropolar fluids. *Journal of Mathematics and Mechanics*, **16**, 1–18 (1966)

[8] Chu, H. M., Li, W. L., and Hu, S. Y. Effects of couple stresses on pure squeeze EHL motion of circular contacts. *Journal of Mechanics*, **22**, 77–84 (2006)

[9] Lin, J. Squeeze film characteristics of finite journal bearings: couple stress fluid model. *Tribology International*, **31**, 201–207 (1998)

[10] Naduvinamani, N. B. and Patil, S. B. Numerical solution of finite modified Reynolds equation for couple stress squeeze film lubrication of porous journal bearings. *Computers and Structures*, **87**, 1287–1295 (2009)

[11] Chang-Jian, C. W., Yau, H. T., and Chen, J. L. Nonlinear dynamic analysis of a hybrid squeeze-film damper-mounted rigid rotor lubricated with couple stress fluid and active control. *Applied Mathematical Modelling*, **34**, 2493–2507 (2010)

[12] Srivastava, V. P. Flow of a couple stress fluid representing blood through stenotic vessels with a peripheral layer. *Indian Journal of Pure and Applied Mathematics*, **34**, 1727–1740 (2003)

[13] Srivastava, L. M. Peristaltic transport of a couple stress fluid. *Rheologica Acta*, **25**, 638–641 (1986)

[14] Umavathi, J. C. and Malashetty, M. S. Oberbeck convection flow of a couple stress fluid through a vertical porous stratum. *International Journal of Non-Linear Mechanics*, **34**, 1037–1045 (1999)

[15] Rani, H. P., Janardhana Reddy, G., and Kim, C. N. Numerical analysis of couple stress fluid past an infinite vertical cylinder. *Engineering Applications of Computational Fluid Mechanics*, **5**, 159–169 (2011)

[16] Alemayehu, H. and Radhakrishnamacharya, G. Dispersion of a solute in peristaltic motion of a couple stress fluid through a porous medium with slip condition. *International Journal of Chemical and Biological Engineering*, **3**, 205–210 (2010)

[17] Hayat, T., Awais, M., Safdar, A., and Hendi, A. A. Unsteady three dimensional flow of couple stress fluid over a stretching surface with chemical reaction. *Nonlinear Analysis*: *Modelling and Control*, **17**, 47–59 (2012)

[18] Stokes, V. K. *Theories of Fluids with Microstructure*, Springer-Verlag, New York/Tokyo (1984)

[19] Carnahan, B., Luther, H. A., and Wilkes, J. O. *Applied Numerical Methods*, John Wiley and Sons, New York (1969)

[20] Von Rosenberg, D. U. *Methods for the Numerical Solution of Partial Differential Equations*, American Elsevier Publishing Company, New York (1969)

[21] Chen, T. S. and Yuh, C. F. Combined heat and mass transfer in natural convection along a vertical cylinder. *International Journal of Heat and Mass Transfer*, **23**, 451–461 (1980)